

# Ship-based and satellite remote sensing cloud retrievals consistency and the quantification of aerosol-cloud interactions

David Painemal<sup>1,2</sup>, Patrick Minnis<sup>1</sup>, Christine Chiu<sup>3</sup>, and Ernie Lewis<sup>4</sup>

<sup>1</sup> Science Systems and Applications, Inc., <sup>2</sup>NASA Langley Research Center, <sup>3</sup> U. of Reading, <sup>4</sup>Brookhaven National Lab.  
david.painemal@nasa.gov

## 1. Introduction

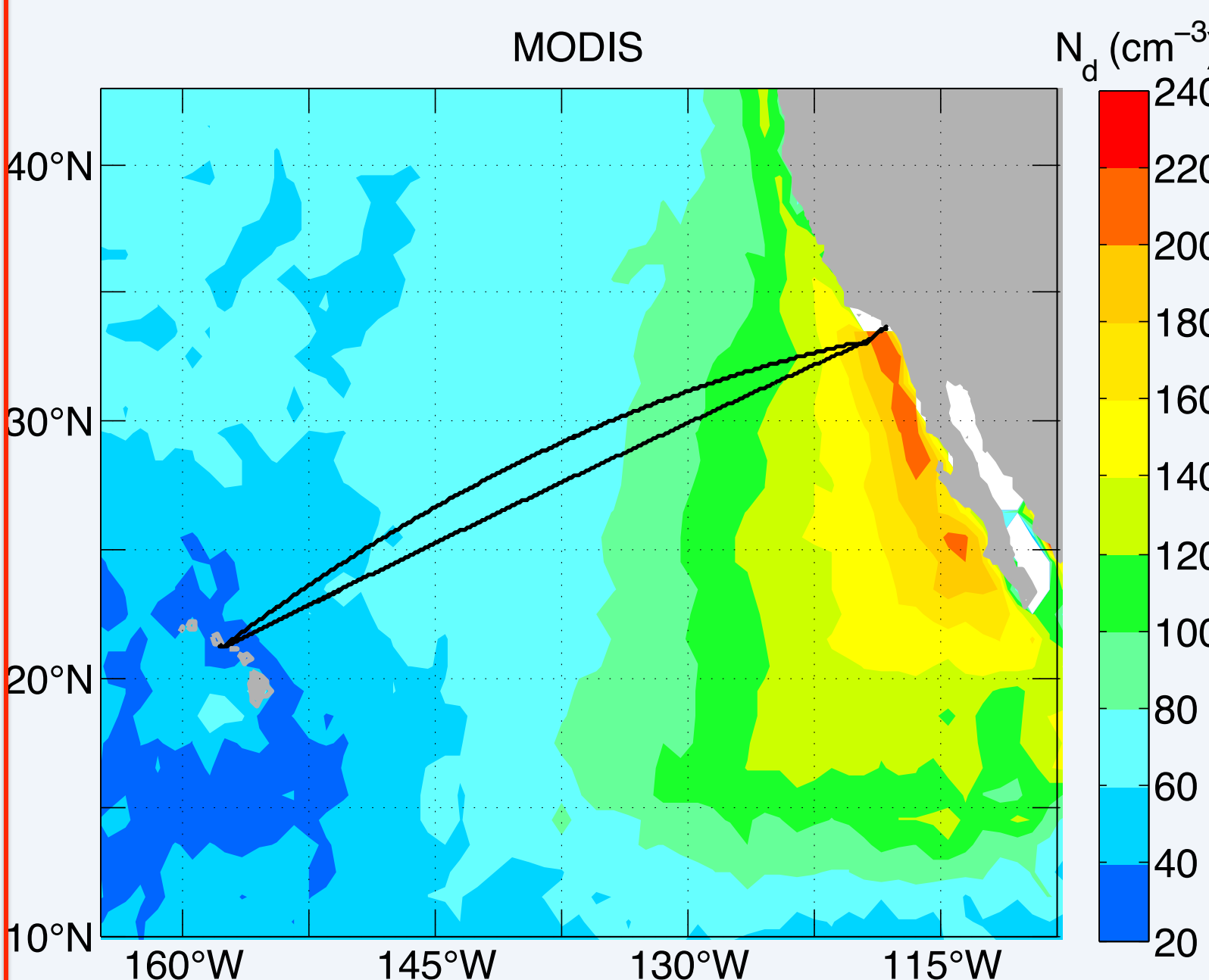


Figure 1: MODIS climatology of cloud droplet number concentration ( $N_d$ ) over the Northeast Pacific. Black solid lines represent the ship transects during MAGIC.

- The northeast (NE) Pacific has been identified as one of the subtropical cloud regimes where microphysical variability driven by aerosols can strongly modify the albedo of the cloud deck [e.g., Painemal and Minnis, 2012]. Satellite-derived cloud droplet number concentration in this region has a notorious westward decrease (Fig. 1).
- The deployment of the second AMF on the container ship, Horizon Spirit, during **MAGIC campaign** presents a unique opportunity to investigate the aerosol variability and cloud-aerosol interactions in marine clouds [Lewis and Teixeira, 2015].
- We evaluate the consistency among different remotely sensed cloud and aerosol properties and analyze their applicability to the quantification of aerosol-cloud interactions during MAGIC.

## 2. Dataset

### Ship-based observations

Liquid water path from a 3-channel microwave radiometer [Cadeddu et al., 2013].

Cloud optical thickness ( $\tau$ ) and effective radius ( $r_e$ ) from a sun-photometer [Chiu et al., 2012].

Aerosols: CCN probe, aerosol size distribution from an Ultra-High Sensitivity Aerosol Spectrometer (UHSAS), aerosol scattering and absorption coefficient from a nephelometer, and a particle soot absorption photometer (PSAP), aerosol backscatter from a high spectral resolution lidar (HSRL)

### Satellite data

$\tau$ ,  $r_e$ , and LWP from the MODerate resolution Imaging Spectroradiometer (MODIS) and geostationary GOES-15 Imager using CERES edition 4 algorithms. MODIS 1km and GOES 4km pixel resolution averaged to a 20 km grid.

## 3. Results

### 3.1. Ship-based vs satellite cloud properties

- Collocated satellite LWP and  $\tau$  agree well with their hourly-mean ship-based counterparts (Fig. 2a and b, respectively).
- Cloud droplet number concentration ( $N_d$ ) assuming adiabaticity [e.g. Painemal and Zuidema, 2013]. This allows to calculate  $N_d$  in terms of (LWP,  $\tau$ ), or (LWP,  $r_e$ ).
- Satellite vs ship-based comparison is best when  $N_d$  is derived from  $\tau$  and LWP.  $\tau$  is typically a more robust ground-based retrieval than  $r_e$  [e.g. Chiu et al. 2012].

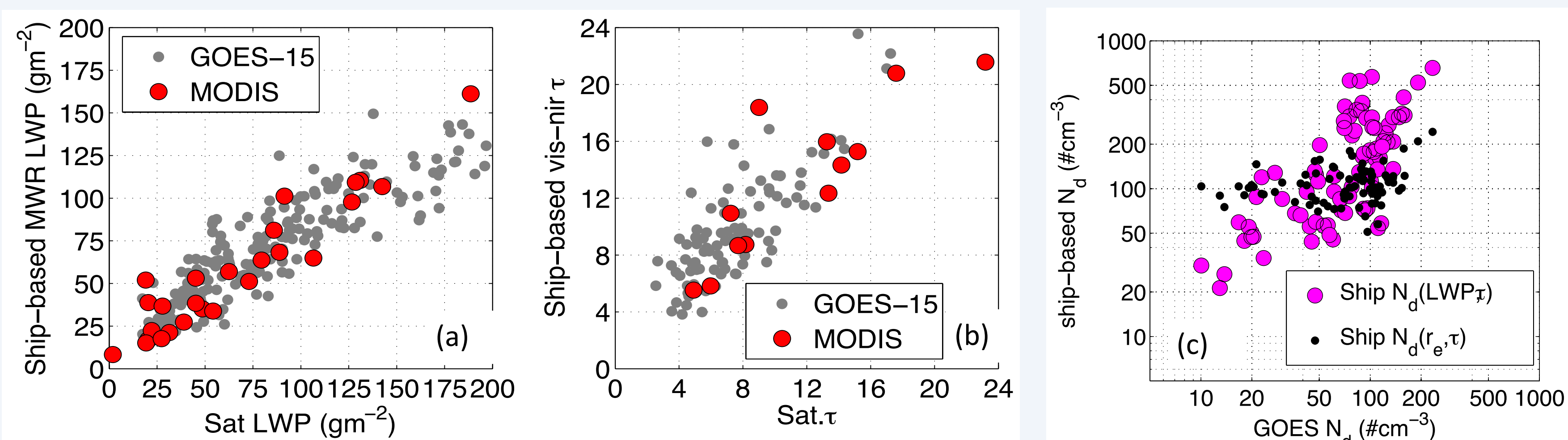


Figure 2: Scatterplot between GOES-15 (gray) and MODIS (red) satellite retrievals against their ship-based counterparts for a) LWP and b)  $\tau$ . c) comparison between ship-based and satellite GOES-15  $N_d$ .

### 3.2. Aerosol proxies

We investigate whether aerosol accumulation mode ( $N_{0.4}$ , UHSAS), dry scattering ( $\sigma_{scatt}$ , nephelometer), and extinction coefficients ( $\sigma_{ext}$ , nephelometer+PSAP) can be used as CCN proxies (0.4% of supersaturation).

- Accumulation mode reproduces the CCN variability (Fig. 3a)
- $\sigma_{scatt}$  and  $\sigma_{ext}$  correlate well with CCN ( $r=0.9$ ), with a modest effect of absorption (Fig. 3b-c).
- York linear fit calculations assuming varying errors ( $\delta$ ) in  $\sigma_{scatt}$  and  $\sigma_{ext}$  and a fixed error in CCN of 10% yield logarithmic slopes between 0.62-0.78, consistent with Shinozuka et al. [2015].

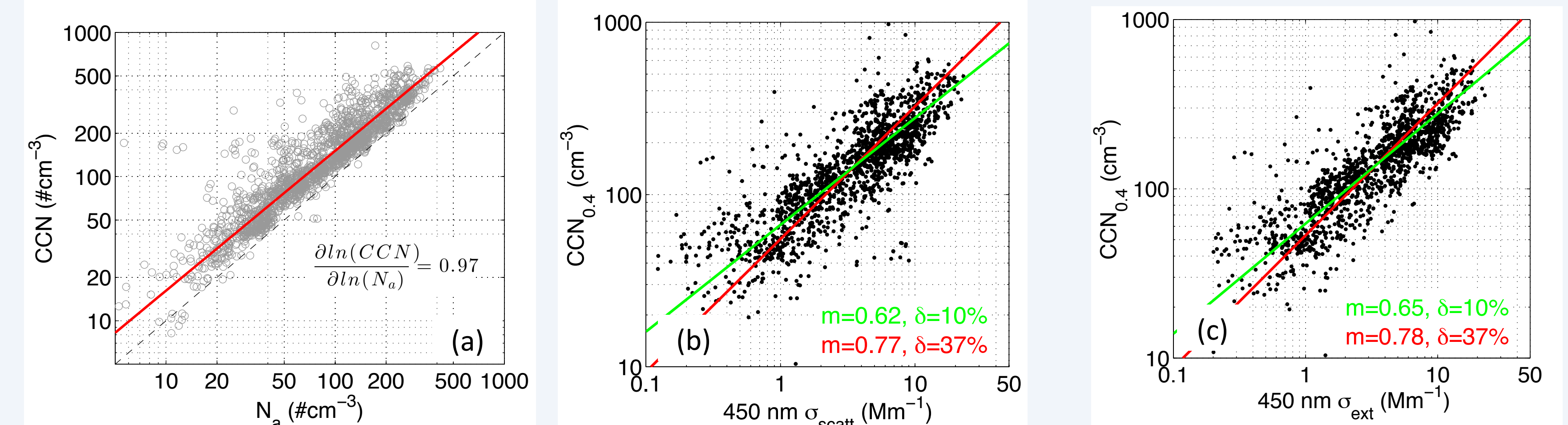
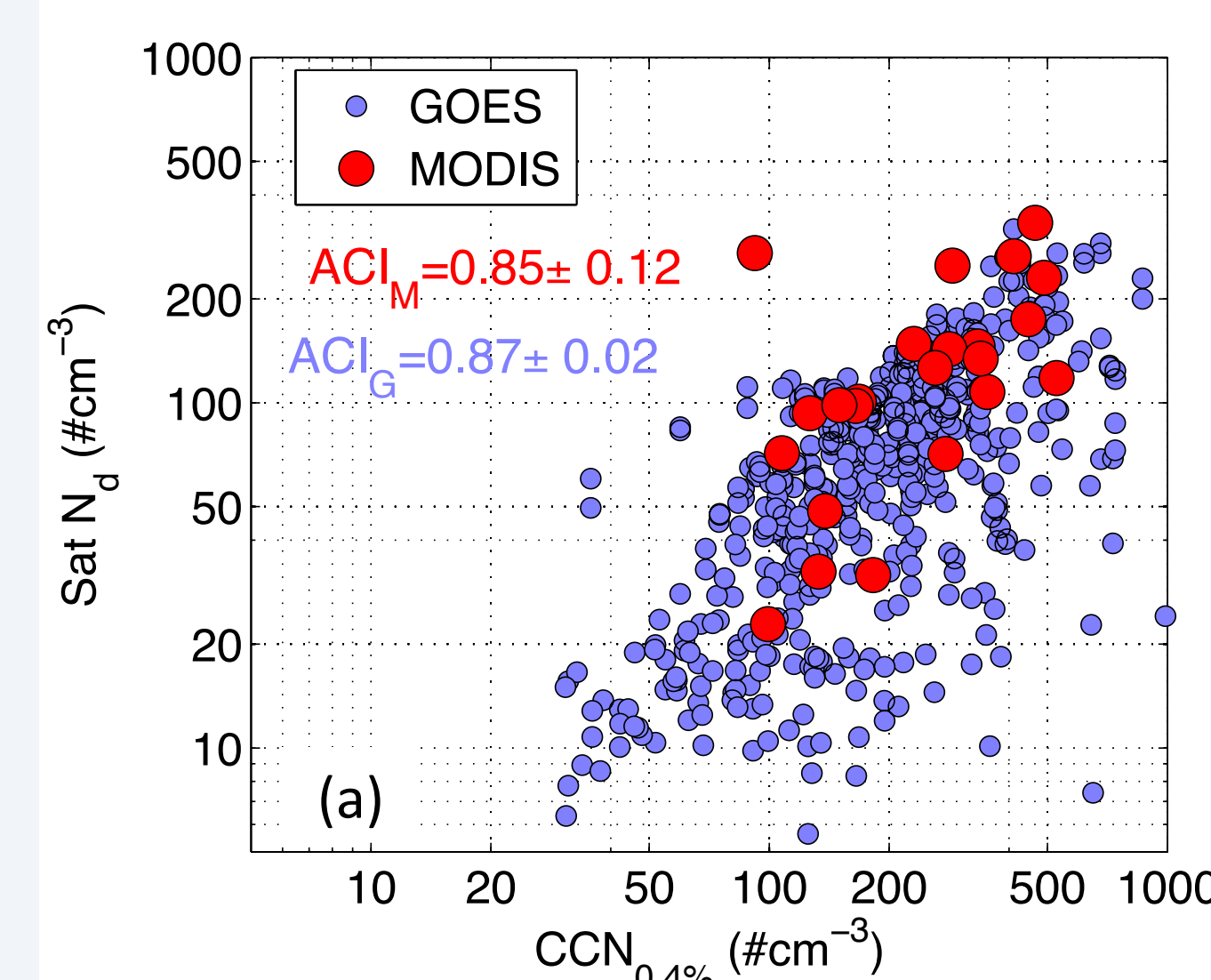


Figure 3: Scatterplot between CCN and a) accumulation mode aerosol  $N_a$ , b) aerosol scattering  $\sigma_{scatt}$  and c) extinction coefficient  $\sigma_{ext}$ . Green and red lines in (b) and (c) are the linear regression using the York method with errors in  $\sigma_{scatt}$  and  $\sigma_{ext}$  of 10% and 37% (10 min standard deviation).

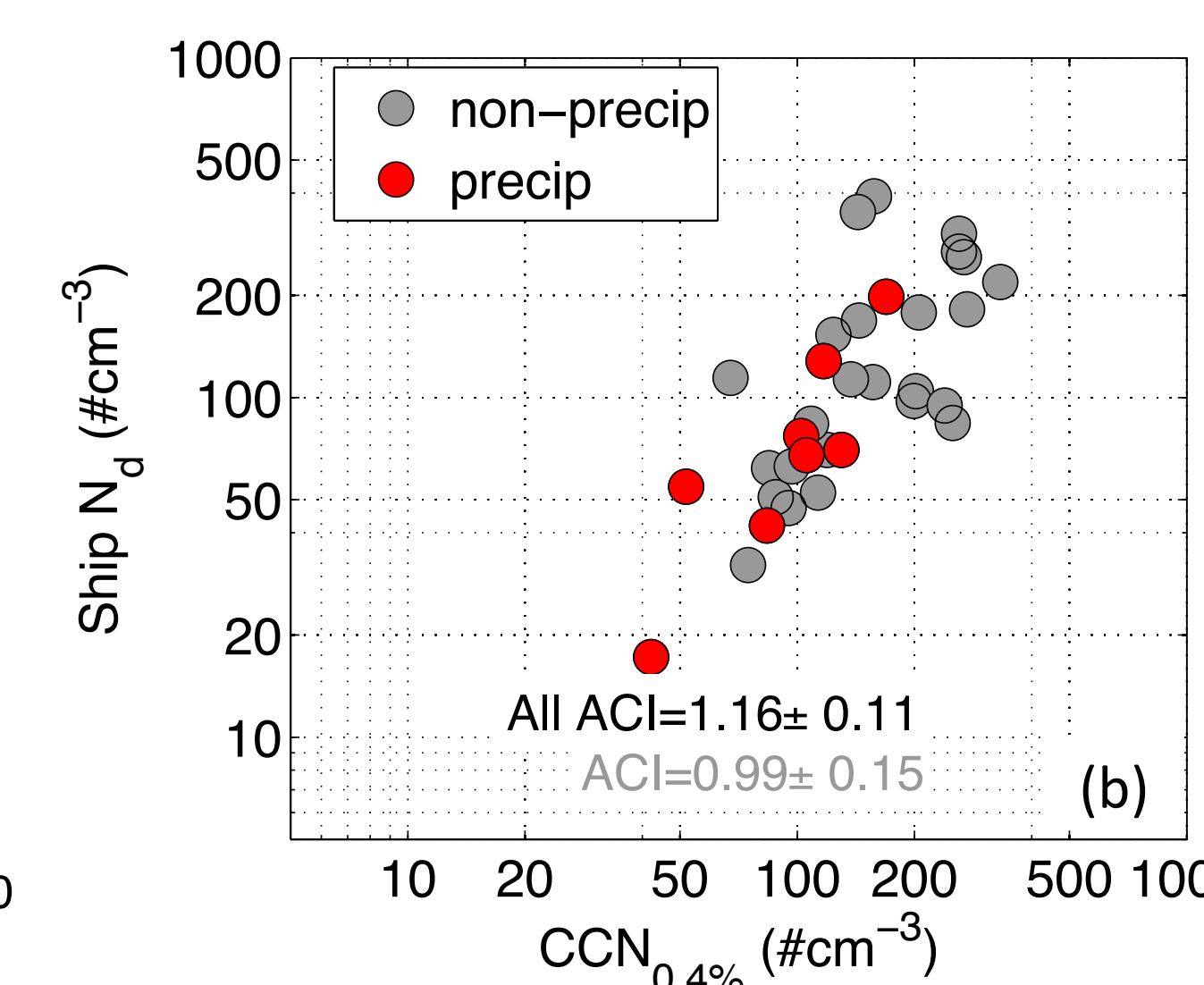
### 3.3. Aerosol-Cloud co-variability

We used a simple metric for quantifying aerosol cloud interactions (ACI):  $ACI = \frac{\partial \ln(N_d)}{\partial \ln(\alpha)}$ , with  $\alpha$  denoting surface observations of CCN or accumulation mode concentration ( $N_a$ ):

#### Satellite-based $N_d$ vs ship-based CCN



#### Ship-based $N_d$ vs ship-based CCN



#### Ship-based $N_d$ vs ship-based $N_a$

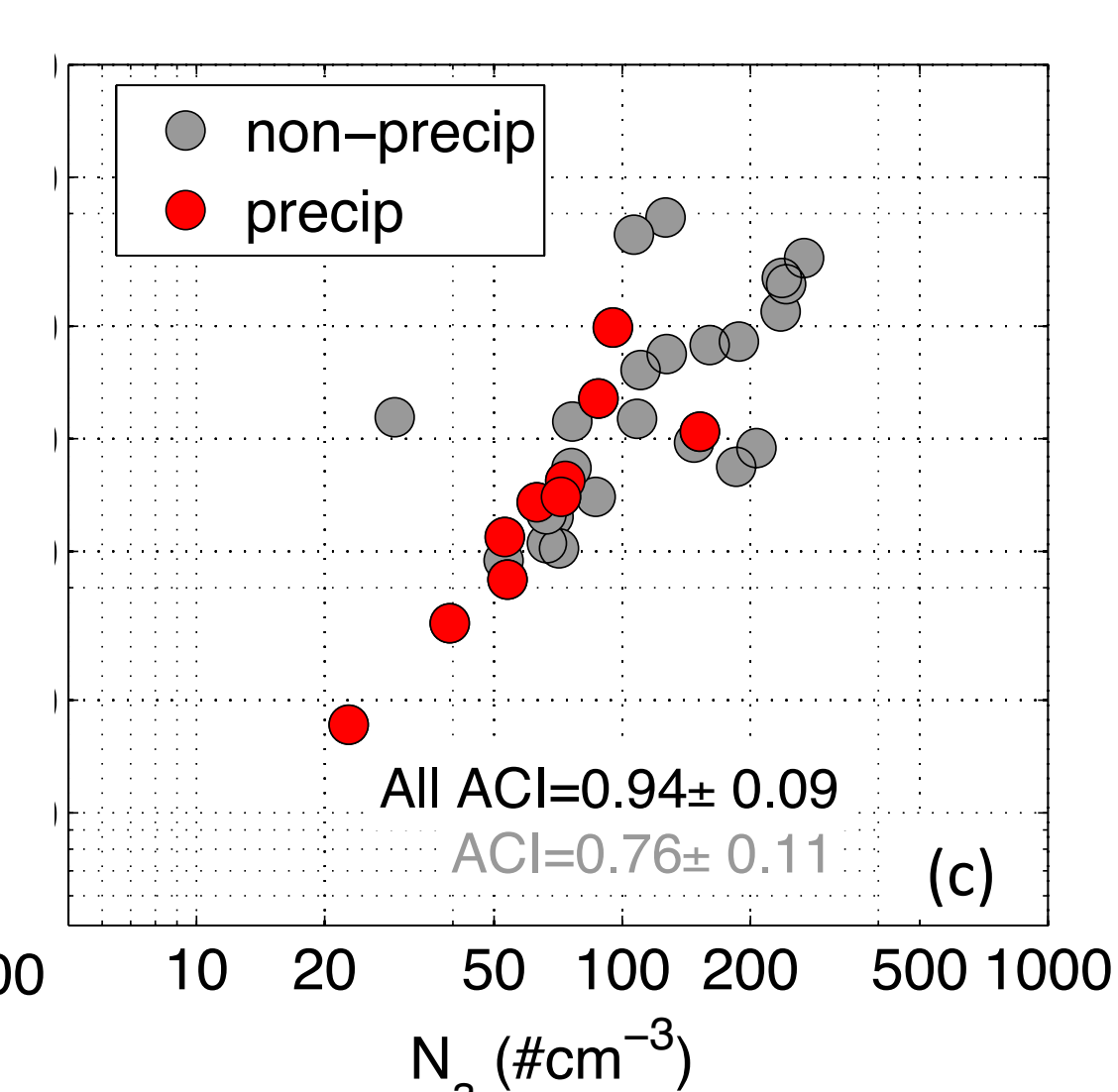
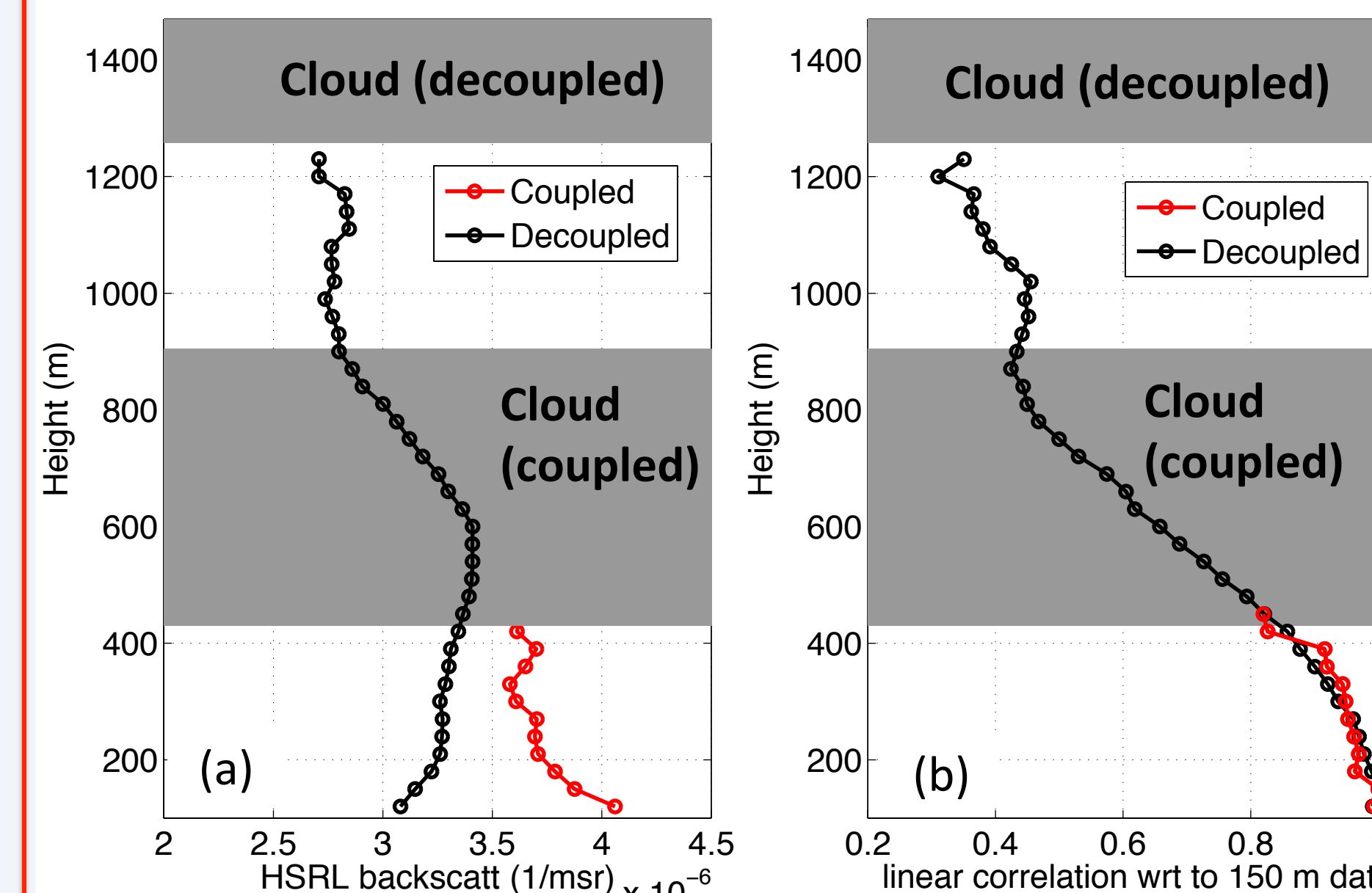


Figure 4: CCN and  $N_d$  vs satellite-based and ship-based  $N_d$  (a and b-c, respectively).

### 3.4. Aerosol vertical structure: preliminary HSRL analysis



- HSRL particle backscatter was used to investigate the aerosol vertical structure during July 2013.
  - **Coupled and decoupled** samples: cloud base height and lifting condensation level difference <200 m and > 400, respectively.
  - Decoupled boundary layers are deeper and backscatter decreases near the cloud base (Fig. 5a).
  - Strong correlations between backscatter at 150 m and those from levels below 400 m. Reduced correlation near the cloud base for the decoupled profile (Fig. 5b).
- Figure 5: a) HSRL mean particulate backscatter, b) correlation between the HSRL backscatter at 150 m at those from level aloft. Red and black are coupled and decoupled cases, respectively.

## 4. Concluding Remarks

- Agreement between satellite and ship-based cloud properties yield consistent  $N_d$ -CCN relationship.
- Accumulation mode aerosols and extinction coefficients are adequate CCN proxies over this region. Extinction-CCN slope <1.0.
- Strong aerosol-cloud interactions consistent with aircraft observations in other marine low clouds regimes.
- Results point to deficiencies in previous satellite-based estimates.
- Information about the aerosol vertical structure might be important in deep (decoupled) boundary layers.

Acknowledgement: ARM-DOE Award DE-SC0011675. CERES program.

#### References:

- Cadeddu et al., 2013, *AMT*, 6, 2359–2372, doi:10.5194/amt-6-2359-2013.
- Chiu et al., 2012, *ACP*, 12, pp. 10313–10329, doi: 10.5194/acp-12-10313-2012
- Lewis and Teixeira (2015), *EOS*, 96, doi:10.1029/2015E0031303.
- Painemal and Minnis, 2012, *JGR*, 117, D06203, doi:10.1029/2011JD017120.
- Painemal and Zuidema, 2013, *ACP*, 13, 917–931, doi: 10.5194/acp-13-917-2013.
- Shinozuka et al., 2015, *ACP*, 15, 7585–7604, doi: 10.5194/acp-15-7585-2015